Effect of the number of blades on the dynamics of floating straight-bladed vertical axis wind turbines

Zhengshun Cheng *[1,2,3], Helge Aagaard Madsen[4], Zhen Gao[1,2,3], and Torgeir Moan[1,2,3]

[1]Department of Marine Technology, Norwegian University of Science and Technology (NTNU), Trondheim, NO-7491, Norway
[2]Centre for Ships and Ocean Structures (CeSOS), NTNU, Trondheim, NO-7491, Norway
[3]Centre for Autonomous Marine Operations and Systems (AMOS), NTNU, Trondheim, NO-7491, Norway
[4]Department of Wind Energy, Technical University of Denmark, Roskilde, 4000, Denmark

September 27, 2016

Abstract

Floating vertical axis wind turbines (VAWTs) are promising solutions for exploiting the wind energy resource in deep waters due to their potential cost-of-energy reduction. The number of blades is one of the main concerns when designing a VAWT for offshore application. In this paper, the effect of blade number on the performance of VAWTs and dynamic behavior of floating VAWTs was comprehensively studied in a fully coupled aero-hydro-servo-elastic way. Three VAWTs with straight and parallel blades, with identical solidity and with a blade number varying from two to four, were designed using the actuator cylinder method and adapted to a semi-submersible platform. A generator torque controller was also designed based on a PI control algorithm. Time domain simulations demonstrated that the aerodynamic loads and structural responses are strongly dependent on the number of blades. In particular, by increasing the number of blades from two to three reduces the variation in the tower base bending moment more significantly than increasing it from three to four. However, the blade number does not significantly affect the generator power production due to the control strategy employed, and the platform motions and tension in mooring lines because of the compliant catenary mooring system.

Key words: Floating vertical axis wind turbine; straight blades; number of blades; aero-hydro-servo-elastic; dynamic response

*Corresponding author. Email address: zhengshun.cheng@ntnu.no Tel.:+47-7359 6004; fax: +47-7359 5528.

1 Introduction

In the last decades, offshore wind turbine installations are experiencing a rapid growth in shallow waters due to the increasing demand for renewable energy production. Most wind turbines deployed are bottom-fixed horizontal axis wind turbines (HAWTs) due to their commercial success onshore or near-shore. However, offshore wind farms are moving towards deeper waters where floating wind turbines are required in countries such as Japan, United States and United Kingdom. Floating HAWTs are now beening widely studied and prototypes have been developed and tested, such as the Hywind demo in Norway, the WindFloat demo in Portugal and the floating wind turbines off the Fukushima coast of northeast Japan.

Floating vertical axis wind turbines (VAWTs) are also a promising alternative to harvest wind energy in deeper waters. Compared with floating HAWTs, floating VAWTs have lower centers of gravity, are independent of wind direction, can provide reduced machine complexity and have the potential of achieving more than 20% cost of energy reductions (Paquette and Barone, 2012). Moreover, floating substructures can help to mitigate the fatigue damages that are suffered by landbased VAWTs (Wang et al., 2016). In addition, floating VAWTs are more suitable for deploying as wind farms than floating HAWTs (Dabiri, 2011), since they are less affected by wake effects. The wake generated by a pair of counter-rotating H-rotors can dissipate more quickly than that of floating HAWTs, allowing them to be installed in wind farms with smaller separations. Thus, increasing efforts are devoted to the development of floating VAWTs, and currently several floating VAWT concepts have been proposed, including the DeepWind (Paulsen et al., 2015), VertiWind (Cahay et al., 2011) and Aerogenerator X (Collu et al., 2014) concepts.

Floating VAWTs can be categorized according to the blade configuration, such as the straight-bladed VAWT, curve-bladed VAWT, helical-bladed VAWT and V-shaped VAWT. A number of studies have been conducted for the straigh-bladed and curved-bladed floating VAWTs to investigate their dynamic response characteristics. Based on a 5 MW two-bladed Darrieus rotor designed in the DeepWind project (Paulsen et al., 2015), Wang et al. (2013) proposed a floating VAWT concept with this rotor mounted on a semi-submersible platform. Fully coupled aero-hydro-servo-elastic simulations were carried out to investigate the stochastic dynamic responses (Wang et al., 2016), effects of second order difference-frequency forces and wind-wave misalignment (Wang et al., 2015), and emergency shutdown process with consideration of faults (Wang et al., 2014). Using the semi-submersible VAWT concept proposed by Wang et al. (2013), Borg and Collu (2015) studied the aerodynamic characteristics of a floating VAWT in the frequency domain. Moreover, the dynamic response characteristic of three floating VAWT concepts with this two-bladed Darrieus rotor mounted on a spar, semi-submersible and TLP floater are investigated by Cheng et al. (2015), and for the spar-type VAWT, a comparative study with the spar-type HAWT is performed to demonstrate the merits and disadvantages in the dynamic responses for each concept (Cheng et al., 2016c). In addition, dynamic analysis of floating VAWT concepts with straight blades are also conducted. Borg et al. (2013) used a wave energy converter as a motion suppression device for a floating VAWT with a two-bladed H-type rotor mounted on a semi-submersible; Borg et al. (2015) studied the long term performance of a three bladed H-rotor mounted on a semi-submersible. However, the method used by Borg et al. (2013, 2015) did not account for the structural elasticity and controller dynamics, and the mooring systems were simplified as springs. Anagnostopoulou et al. (2015) performed the concept design and dynamic analyses of a floating VAWT with a three-bladed rotor mounted on a semi-submersible for power supply to offshore Greek islands; however, the wind loads acting on the rotor is very simplified in this study.

The aforementioned dynamic analysis of floating VAWTs considered the curve-bladed rotor with two blades, and the straight-bladed rotor with two or three blades. Significant 2P (two per revolution) effects are revealed and demonstrated for the two-bladed floating VAWTs. As a matter of fact, choosing the number of blades is an important issue when designing a VAWT for offshore application with given blade type, since the number of blades may significantly affect the aerodynamic performance of VAWTs and dynamic response characteristics of floating VAWT systems. The effect of the number of blades on the aerodynamic performance of VAWTs with straight-bladed and curve-bladed blades has been numerically and experimentally studied by several researchers. Considering a set of curve-bladed VAWTs with constant solidity and different blade number that varies from one to four, the impact of the number of blades on the aerodynamic loads was numerically estimated by Bedon et al. (2015) based on the double multiple streamtube method. The considered VAWT was originally developed in the DeepWind project (Paulsen et al., 2015), which was mounted on a floating platform. Li et al. (2015) evaluated the effect of blade number on the aerodynamic forces on a straight-bladed VAWT using the wind tunnel experiment. Considering the number of blades varying from two to five, the tangential and normal forces were quantitatively studied as a function of azimuth angle. However, these studies only discuss the effect of the number of blades from the aerodynamic point of view and do not reveal its potential impact on the dynamic responses of floating VAWTs in a fully coupled way. These dynamic responses include the generator power production, platform motions, structural loads and tension in mooring lines etc. To which extent these dynamic responses could be influenced by the number of blades for floating VAWTs is still unknown and of great interest.

This study aims to demonstrate the effect of the number of blades on the dynamic responses of floating VAWTs by a series of fully coupled time domain simulations. Firstly, three straight-bladed VAWTs with identical solidity and different number of blades are designed using the actuator cylinder flow method. The number of blades varies from two to four. A generator torque controller is also designed based on the control strategy established by Cheng et al. (2016b). These three VAWTs are then adapted to a semi-submersible platform to achieve three floating VAWTs. Using the fully coupled code SIMO-RIFLEX-AC (Cheng et al., 2016b), a series of load cases are conducted to identify the floating VAWT systems and to illustrate the discrepancy in the dynamic responses of these three floating VAWTs. This study systematically demonstrates the effect of the number of blades on the dynamic responses of floating VAWTs and can serve as a basis for the design of floating VAWTs.

2 Methodology

In this study, an aerodynamic code based on the actuator cylinder (AC) flow model, initially developed by Madsen (1982) and implemented and modified by Cheng et al. (2016a), was used to design three straight-bladed VAWTs and a corresponding generator-torque controller. Compared with the conventional double multi-streamtube method (Paraschivoiu, 2002), the AC method predicts more accurate aerodynamic loads with similar computational efficiency (Ferreira et al., 2014; Cheng et al., 2016a). The code SIMO-RIFLEX-AC developed by Cheng et al. (2016b) was later used to conduct fully coupled aero-hydro-servo-elastic time domain simulations. The relevant theories for the AC and SIMO-RIFLEX-AC code are briefly summarized in this section.

2.1 Actuator cylinder flow method

The AC method is a 2D quasi-steady flow model proposed by Madsen (1982). The model extends the actuator disc concept to an actuator surface coinciding with the swept area of the 2D VAWT. In the AC model, the normal and tangential forces resulting from the blade forces are applied on the flow as volume force perpendicular and tangential to the rotor plane, respectively. The induced velocities are thus related to the volume force based on the continuity equation and Euler equation. The induced velocity can be divided into a linear part and a nonlinear part; the linear part can be computed analytically given the normal and tangential loads . However, it is to some extent time-consuming to compute the nonlinear solution directly. A simple correction is therefore introduced to make the final solution in better agreement with the fully nonlinear solution (Madsen et al., 2013).

The developed AC code (Cheng et al., 2016a) includes the effect of normal and tangential loads when calculating the induced velocity, uses a more physical approach to represent the normal and tangential loads and a new modified linear solution. The effect of dynamic stall was also incorporated using the Beddoes-Leishman model. The AC code was validated by comparison with other numerical models and experimental data and was found to be accurate (Cheng et al., 2016a).

2.2 Fully coupled numerical method

The developed AC code (Cheng et al., 2016a) was integrated with the SIMO (MARINTEK, 2012b) and RIFLEX (MARINTEK, 2012a) codes to achieve a fully coupled aero-hydro-servo-elastic code, namely SIMO-RIFLEX-AC (Cheng et al., 2016b), for numerical modeling and dynamic analysis of floating VAWTs. The SIMO (MARINTEK, 2012b) and RIFLEX (MARINTEK, 2012a) codes were developed by MARINTEK and have been widely used in the offshore oil and gas industry. The SIMO-RIFLEX-AC code is capable of accounting for the turbulent wind inflow, aerodynamics, hydrodynamics, structural dynamics, control system dynamics and mooring line dynamics. It integrates three computer codes: SIMO (MARINTEK, 2012b) computes the hydrodynamic loads acting on the platform hull; RIFLEX (MARINTEK, 2012a) models the blades, tower, shaft, struts and mooring lines using flexible finite elements and provides links to an external controller and AC; and AC calculates the aerodynamic loads acting on the blades. Moreover, a generator torque controller based on the proportional-integral (PI) control algorithm is implemented to regulate the rotor rotational speed. The SIMO-RIFLEX-AC code has been verified by a series of numerical comparisons with the codes HAWC2 and SIMO-RIFLEX-DMS (Cheng et al., 2016b).

In this study, a semi-submersible supporting straight-bladed VAWTs was studied. The aerodynamic loads acting on the blades were calculated based on the AC method as described above, and the effect of the wind shear and turbulence, dynamic inflow and dynamic stall was all taken into account. But the effect of the tip loss, tower shadow as well as the drag forces on the struts and tower was neglected.

The hydrodynamic loads acting on the semi-submersible hull was represented using a combination of potential flow and Morison's equation. Added mass, radiation damping and first order wave excitation forces were obtained from a potential flow model and applied in the time domain using the convolution technique (Faltinsen, 1995). Additional viscous damping on the hull was included using the Morison's formula. Morison's formula was also applied to the brace and mooring lines that were not included in the potential flow model.

In the structural model, the semi-submersible including the braces were represented as a rigid body; the blades, struts, tower and shaft were modeled using nonlinear beam elements; and the mooring lines were considered as nonlinear bar elements. A very short tower close to the tower base was used to connect the rotating shaft and semi through a flexible joint. The equations of motions were solved in the time domain using the Newmark-β integration method ($\beta = 0.256$, $\gamma = 0.505$) (Bachynski, 2015). Structural damping was included through global proportional Rayleigh damping terms for all beam elements.

3 Floating VAWT models

3.1 Design of straight bladed VAWTs

Considering a straight bladed VAWT with a radius of R and height of h, the power can be expressed as (Brusca et al., 2014)

$$P = \frac{1}{2}\rho U_w^3 \left(2Rh\right) C_p \tag{1}$$

where ρ is the air density, U_w is the wind speed, and C_p is the power coefficient. For a specific airfoil type, the power coefficient C_p is a function of the tip speed ratio λ, rotor solidity σ and Reynolds number Re, which are defined as follows.

$$\lambda = \frac{\omega R}{U_w} \tag{2}$$

$$\sigma = \frac{Bc}{R} \tag{3}$$

$$Re = \frac{cV_{rel}}{\nu} \tag{4}$$

in which B is the blade number, c is the chord length, ν is the kinematic air viscosity, and V_{rel} is the relative velocity seen by the airfoil. Assuming the aspect ratio γ is given by $\gamma = h/R$, therefore the power can be rewritten as

$$P = \frac{\rho\omega^3 R^5 \gamma C_p(\lambda, \sigma, Re)}{\lambda^3} \tag{5}$$

In this study three 5MW VAWTs with straight blades and the NACA 0018 airfoil, as shown in Figure 2, were designed. Eq. 5 shows that the power coefficient C_p is one of the crucial parameters and should be firstly determined. Large megawatt VAWTs usually operate at very high Reynolds number. Figure 1 shows the power coefficient C_p plotted against the tip speed ratio λ as a function of rotor solidity σ for the NACA 0018 airfoil at Reynolds number of $8 \sim 10 \times 10^6$. It should be noted here that the Reynolds number experienced by the airfoil at a specific position along the blade varies periodically when the rotor rotates. In this study it is assumed that such variation in the Reynolds number will not cause much changes in the corresponding lift and drag coefficients for the NACA 0018. Due to the consideration of solidity and power coefficient of large megawatt VAWTs in reality, such as the design in the FP7 H2OCEAN project (Borg et al., 2015), the solidity of $\sigma = 0.20$ is chosen, which has a $C_{pmax} = 0.50$ corresponding to $\lambda = 3.0$.

Assuming that the rated wind speed is 14.0 m/s and the aspect ratio is set to be 2.05, three optimal designs for a rated power of 5.3 MW are given in Table 1. The height of tower top, i.e. the vertical center of blades, is assumed to be 79.78 m. The aerodynamic power is estimated considering the wind shear with a power coefficient of 0.14 according to the IEC 61400-3 (IEC, 2005). In the design process, the chord length is reduced with increasing

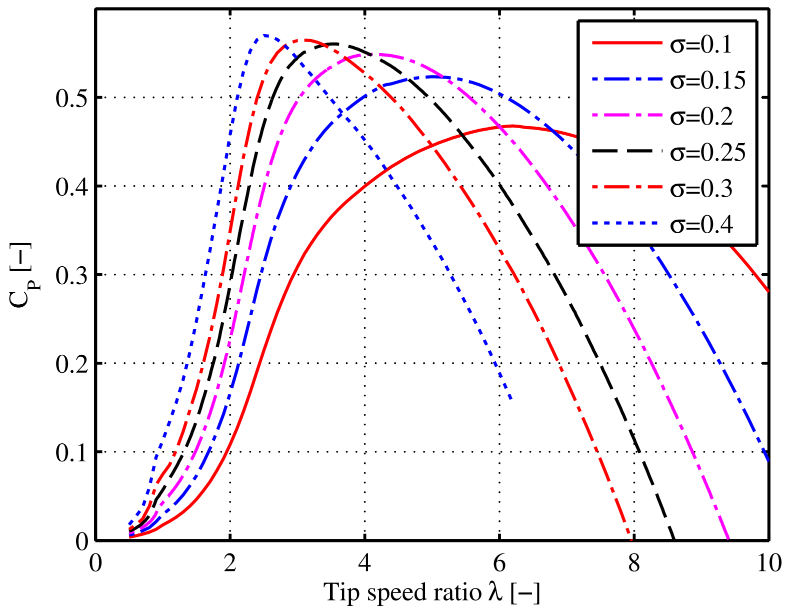

Figure 1: Power coefficient of a VAWT with straight blades and symmetric airfoil NACA 0018 at high Reynolds number of $8 \sim 10 \times 10^6$ for different rotor solidity $\sigma = \frac{Bc}{R}$.

number of blades so as to keep the solidity constant. This can also cause a change in Reynolds number and thus affect the lift and drag coefficients, but the impact on the total aerodynamic loads and power is assumed to be small. In addition, despite the same solidity number, the mean thrust coefficients have small variation because of the different number of blades. Since the modified linear solution in the AC method is sensitive to the mean thrust coefficient, the computed rated power does therefore show small deviation from the value of 5.3 MW.

Table 1: Main parameters of the designed VAWTs

	H2	H3	H4
Rated power [MW]	5.21	5.30	5.35
Blade number [-]	2	3	4
Rotor radius [m]	39.0	39.0	39.0
Height [m]	80.0	80.0	80.0
Chord length [m]	4.05	2.7	2.03
Tower top height [m]	79.78	79.78	79.78
Aerofoil section	NACA 0018	NACA 0018	NACA 0018
Cut-in, rated and cut-out wind speed [m/s]	5.0, 14.0, 25.0	5.0, 14.0, 25.0	5.0, 14.0, 25.0
Rated rotational speed [rad/s]	1.08	1.08	1.08

3.2 Description of landbased and floating VAWT models

In this study, three straight-bladed floating VAWTs with a semi-submersible floater are considered. For the straight-bladed rotors, the structural properties of the blades, struts, tower and shaft were determined on the basis of the Deepwind rotor (Paulsen et al., 2015), which was a 5 MW Darrieus rotor. The blades of the designed straight-

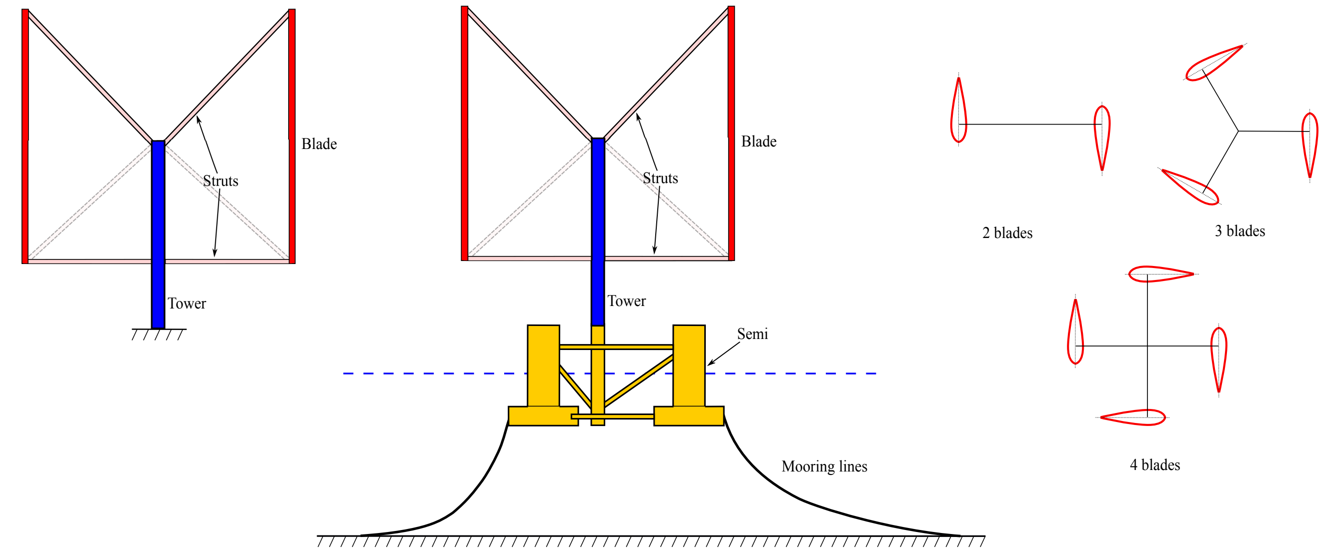

(a) Straight-bladed landbased VAWTs (b) Straight-bladed floating VAWTs (c) Top view of the blades

Figure 2: The landbased and floating straight-bladed VAWTs with different number of blades.

bladed rotors and Deepwind rotor both used the same NACA 0018 airfoil, but they differed in the chord length. It was thus assumed that the structural properties of the blades, such as the mass per unit length, axial and bending stiffness, are related to a length scale that is determined using the chord length. In this study, the blades, instead of struts, are our concern. To avoid large deformation in the blades at high wind load conditions, the stiffness of the blades and struts was increased. The stiffness of the tower and shaft remained the same as the Deepwind design. Actually in a realistic design, the struts might be different from the present ones and additional struts, as the dash line shown in Figure 2, could be constructed. The mass properties of the three rotors are given in Table 2.

The OC4 semi-submersible (Robertson et al., 2012) , which was originally designed to support the NREL 5 MW wind turbine (Jonkman et al., 2009), was used to support the three straight-bladed VAWTs. The considered water depth was assumed to be 200 m. The same semi-submersible was used to support the 5 MW Darrieus Deepwind rotor and studied by Cheng et al. (2015) and Wang et al. (2016). Due to the difference in the rotor mass, the ballast of the semi-submersible was adjusted to maintain the same draft and displacement when supporting three different VAWTs. Properties of the three floating VAWT systems are given in Table 2. More details about the semi-submersible and catenary mooring system are given by Robertson et al. (2012). The generator was assumed to be located at the tower base and its mass was incorporated in the platform mass. Since the difference in the rotor mass between the NREL 5 MW wind turbine and three designed rotors is small compared to the displacement of the semi-submersible, it is therefore assumed that such modification will not significantly affect the hydrostatic and hydrodynamic performance of each floater.

Although the structural properties of rotors and the substructure is not optimal from an economic point of view, they are sufficient to demonstrate and reveal the effect of the number of blades on the dynamics of floating VAWTs.

Table 2: Properties of the floating VAWT systems

	Semi H2	Semi H3	Semi H4
Water depth [m]	200	200	200
Draft [m]	20	20	20
Diameter at mean water line [m]	12.0/6.5	12.0/6.5	12.0/6.5
Rotor mass, including blades, struts, tower and shaft [ton]	350.1	315.3	287.7
Center of mass for rotor [m]	(0, 0, 51.03)	(0, 0, 48.14)	(0, 0, 45.34)
Platform mass, including ballast and generator [ton]	13761.3	13796.1	13823.7
Center of mass for platform [m]	(0, 0, -13.44)	(0, 0, -13.43)	(0, 0, -13.43)
Buoyancy at the equilibrium position [kN]	139816	139816	139816
Center of buoyancy [m]	(0, 0, -13.15)	(0, 0, -13.15)	(0, 0, -13.15)

3.3 Control strategy for the landbased and floating VAWTs

In this section, a generator-torque controller is designed for the above VAWTs. Cheng et al. (2016b) demonstrated the typical relationship between the reference rotational speed and wind speed for a typical floating VAWT system and identified two control strategies, namely the baseline controller and improved controller, in terms of the target in the region above the rated wind speed. Herein the improved controller was adopted.

Considering the 3-bladed VAWT, the rotor power is plotted against the rotational speed as a function of wind speed, as shown in Figure 3. For wind speeds below the rated wind speed, the designed rotational speed is determined by maximizing the power capture. Regarding wind speeds ranging from 5-10.5 m/s, the rotational speed is chosen to make the rotor operating at the optimal tip speed ratio. Moreover for wind speeds ranging from 10.5-14 m/s, the rotational speed is set to be the rated rotational speed. Therefore the optimized curve rotational speed can be obtained for wind speeds below the rated one.

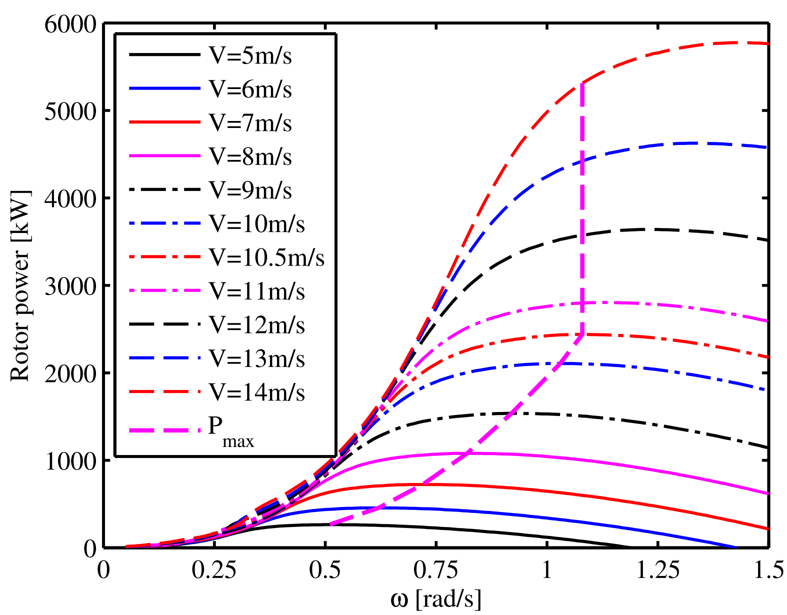

Figure 3: The mean aerodynamic power as a function of the rotational speed and wind speed.

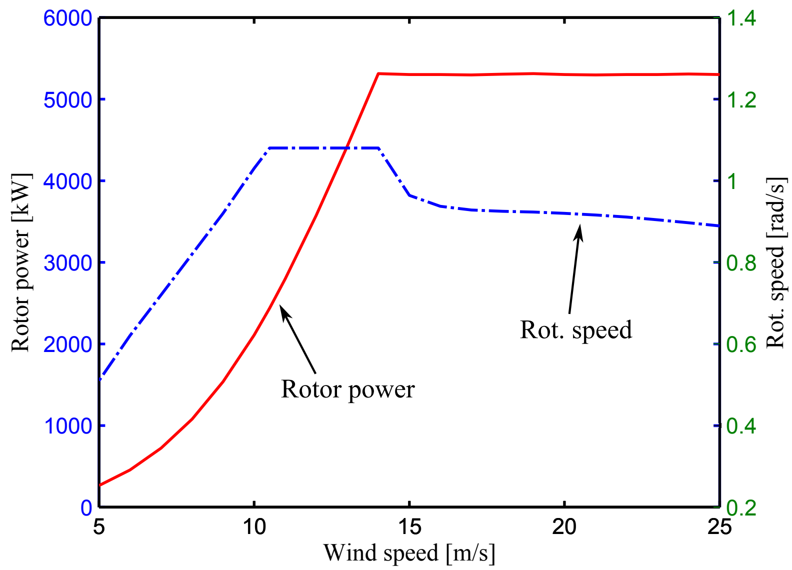

Figure 4: The mean rotor power and rotational speed as a function of wind speed for the improved control strategy.

With respect to wind speeds above the rated one, the improved controller that maintains the mean rotor power approximately constant is applied. Given a wind speed, the desirable rotational speed is computed to make the mean aerodynamic power achieve a prescribed value, for instance 5.3 MW in this study. In this way the designed rotational speed is obtained as a function of wind speed as demonstrated in Figure 4.

In the implementation of the controller, the generator rotational speed and electric torque are measured and low-pass filtered. The controller aims to minimize the error between the measured and filtered rotational speed Ω_{mea} and the reference rotational speed Ω_{ref},

$$\Delta\Omega = \Omega_{mea} - \Omega_{ref} \tag{6}$$

in which the reference rotational speed Ω_{ref} is determined on the basis of a look-up table showing the relationship of the filtered electric torque and reference rotational speed for wind speeds below the rated one; while for wind speed above the rated one, it is determined according to a look-up table of the low-pass filtered wind speed and reference rotational speed.

The rotational speed error $\Delta\Omega$ is then fed through the proportional, integral and derivative paths to obtain an updated value of the required electric torque, as follows,

$$T(t) = K_G\left(K_P\Delta\Omega(t) + K_I\int_0^t \Delta\Omega(\tau)d\tau + K_D\frac{d}{dt}\Delta\Omega(t)\right) \tag{7}$$

in which K_G is the generator stiffness, and K_P, K_I and K_D are the proportional, integral and derivative gains, respectively. In this study, the value of K_G, K_P, K_I and K_D were determined with reference to the controller developed by Merz and Svendsen (2013) for the DeepWind 5MW Darrieus rotor.

The aforementioned controller is determined using the 3-bladed VAWT. It is also applicable to the 2- and 4-bladed VAWTs, as illustrated in Figure 6. Figure 6 shows the mean value of the generator power production of three equivalent landbased VAWTs and three floating VAWTs considered in the steady wind conditions. Description of the landbased and floating VAWTs can refer to section 3.2. Obviously all the mean generator power of the three rotors follow the pre-calculated power curve very well. Therefore, the designed controller was applied for the VAWTs in all simulations.

4 Load cases and environmental conditions

A series of load cases (LCs) were defined for the floating VAWT system and used in the time domain simulations, as given in Tables 3 and 4. LC1 and LC2 are free decay and white noise wave cases, respectively. They are used to identify the three floating VAWT systems and capture the difference in terms of natural periods of rigid body motions and response amplitude operators (RAOs). Those differences should be small in order to reveal the essential effect of the number of blades on the dynamics of floating VAWTs. LC3 and LC4 are the steady wind only cases and the turbulent wind and irregular wave cases, respectively. The wind and wave are correlated and directionally aligned. The difference between the 2, 3 and 4-bladed VAWT is mainly related to the aerodynamic loads, not very much to the wave loads. Moreover, the aerodynamic loads on a VAWT is not dependent on the wind direction. Therefore, the effect of wind-wave misalignment will not change their dynamic performances significantly. But the quantitative effect should be studied in the future.

Table 3: Load cases: free decay and white noise

Load cases (LCs)		Response	Wind Cond.	Wave Cond.
LC1	Decay	Decay (Surge, heave, pitch and yaw)	-	Calm water
LC2	White noise	RAO	-	White noise

The normal wind profile (NWP) was applied in the steady wind conditions, in which the wind profile is the average wind speed as a function of height z above mean sea level (MSL) and is given as follows

$$U(z) = U_{ref}\left(\frac{z}{z_{ref}}\right)^{\alpha} \tag{8}$$

where U_{ref} is the reference wind speed, z_{ref} is the height of reference wind speed and α is the power law exponent. In this study z_{ref} was set to be 79.78 m, which is the vertical center of blades above MSL. The value of α was chosen to be 0.14 for the floating wind turbines according to IEC 61400-3 (IEC, 2005). For turbulent wind conditions, the TurbSim (Jonkman, 2009) was used to generate the three dimensional turbulent wind field according to the Kaimal turbulence model for IEC Class C. Regarding the irregular wave conditions, the irregular wave history was generated using the JONSWAP wave model. The significant wave height and peak period were set based on their correlation with wind speed for the Statfjord site in the northern North Sea (Johannessen et al., 2002).

In the turbulent wind and irregular wave LCs, each simulation lasted 4600 s and corresponded to a one-hour dynamic analysis, since the first 1000 s was removed to eliminate the start-up transient effects. Five identical and independent one-hour simulations with different seeds for the turbulent wind and irregular waves were carried out for each LC to reduce the stochastic variations. The mean value and standard deviation of the dynamic responses were obtained by averaging the mean values and standard deviations of five one-hour ensembles.

Table 4: Load cases: wind and wave cases

	U_W [m/s]	H_S [m]	T_P [s]	T_I [-]	Wave Cond.	Simulation Length [s] *
LC3.1	5	-	-	0	-	800
LC3.2	8	-	-	0	-	800
LC3.3	10	-	-	0	-	800
LC3.4	12	-	-	0	-	800
LC3.5	14	-	-	0	-	800
LC3.6	18	-	-	0	-	800
LC3.7	22	-	-	0	-	800
LC3.8	25	-	-	0	-	800
LC4.1	5	2.10	9.74	0.224	Irreg. wave	3600
LC4.2	8	2.55	9.86	0.174	Irreg. wave	3600
LC4.3	10	2.88	9.98	0.157	Irreg. wave	3600
LC4.4	12	3.24	10.12	0.146	Irreg. wave	3600
LC4.5	14	3.62	10.29	0.138	Irreg. wave	3600
LC4.6	18	4.44	10.66	0.127	Irreg. wave	3600
LC4.7	22	5.32	11.06	0.121	Irreg. wave	3600
LC4.8	25	6.02	11.38	0.117	Irreg. wave	3600

* Net simulation time for stochastic wave and wind conditions, i.e. removal of transient start-up.

5 Results and discussions

5.1 Identification of the properties of floating VAWT systems

A series of numerical simulations were carried out to identify the floating VAWT systems, including the eigen-frequencies of equivalent landbased VAWTs, the natural periods of rigid-body motions of floating VAWTs and the RAOs of floating VAWTs subject to wave loads.

The eigen-frequencies and corresponding eigen modes of the equivalent landbased VAWTs were estimated using the code SIMO-RIFLEX-AC. The eigenvalue problems were solved using the Lanczos' method. The rotors were assumed to be parked and the effects of aerodynamic loads and rotation on the eigen-frequencies and eigen-modes were not considered here. The results show that the two lowest eigen-frequencies of the 2-, 3- and 4-bladed rotors are located outside of the corresponding 2P, 3P and 4P regions, respectively, which indicates that the resonant modes of the rotor will not be excited during the normal operation.

Free decay tests in calm water were carried out using the code SIMO-RIFLEX-AC to estimate the natural periods of rigid body motions for the three floating VAWTs. In the free decay tests, the wind turbines were parked in the position as shown in Figure 2 and were not subjected to the aerodynamic loads. Here the influence of the rotor azimuth angle when parked on the pitch and roll natural periods was neglected since the influence was very small. The results are given in Table 5. These three floating VAWTs have identical draft and displacement and employ the same mooring system, the natural periods in surge, sway and heave motions are thus almost the same. In addition, since the three floating VAWTs have nearly the same rotor masses and the rotor masses are small compared to the displacement, the natural periods in pitch, roll and yaw motions are also close to each other.

The RAOs of floating VAWTs were estimated using the white noise technique. Cheng et al. (2015) stated

Table 5: Natural periods of rigid body motions for the three floating VAWTs

	Semi H2	Semi H3	Semi H4
Surge/Sway [s]	113.15	113.15	113.15
Heave [s]	17.04	17.04	17.04
Pitch/Roll [s]	21.17	20.68	20.32
Yaw [s]	80.38	80.44	80.49

that the white noise technique can capture the natural frequency of rigid-body motions precisely and predict all RAOs accurately except at the resonant frequency of each mode. The white noise waves were created using the fast Fourier transform (FFT) with a frequency interval $\Delta\omega$=0.005 rad/s. In the white noise simulations, the wind turbines were parked as in the free decay tests. The surge and pitch RAOs of the three floating VAWTs are shown in Figure 5. It can be observed that the natural periods captured by the white noise technique agree well with those from the free decay tests. Moreover, the surge and heave RAOs for the three floating VAWTs agree very well over a wide range of frequencies; while visible discrepancy lies in the pitch RAO, especially at the pitch resonant frequency. This is due to the different moment of inertia in pitch of the three floating VAWTs. When adapting the three rotors with different mass to the semi, the ballast of the semi was adjusted to achieve the same draft and displacement for the three floating VAWTs. Consequently, the moments of inertia in pitch and roll of the three floating VAWTs differ, and the pitch natural frequency and pitch resonant response exhibit slight differences.

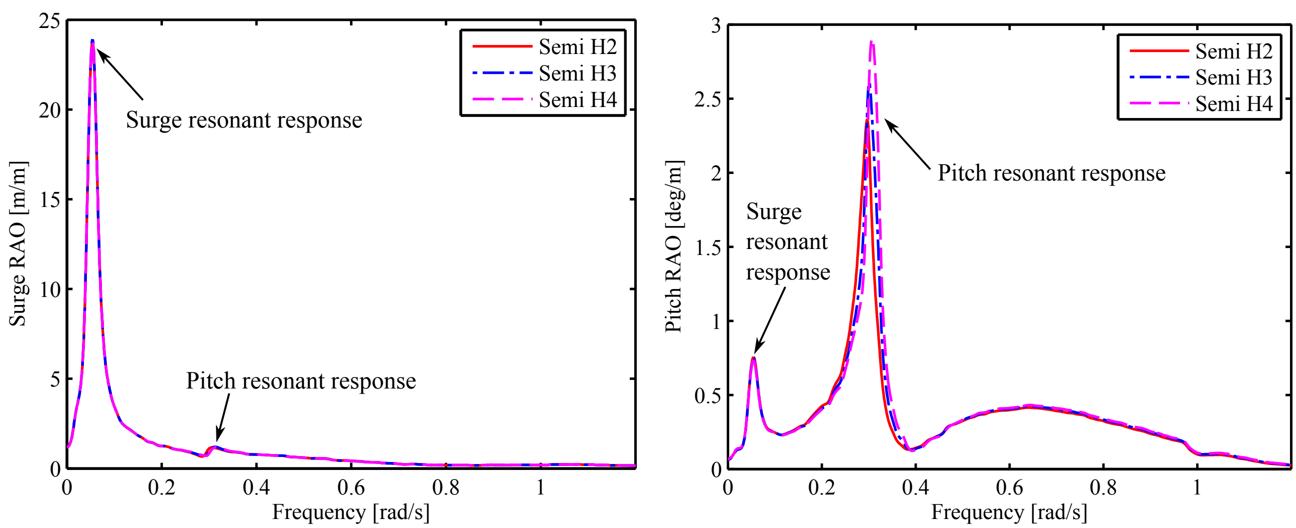

Figure 5: Surge and pitch RAOs of the three floating VAWTs for wave loads.

5.2 Steady wind conditions

The steady wind LCs were used to verify the robustness of the designed controller, and to illustrate the difference between landbased and floating straight-bladed VAWTs with different number of blades.

The robustness of the controller has been investigated and shown in Figure 6. The landbased and floating VAWTs can all achieve the pre-calculated power curve at a given wind speed. Figure 6 also presents the mean thrust of the landbased and floating VAWTs. An example of the time history of the thrust and side force acting on the rotor for the three floating VAWTs are shown in Figure 7. In general the mean thrust of the landbased and floating VAWTs are close to each other, and the small difference, especially in high wind speeds, is mainly due to two possible reasons: one is that the effect of dynamic stall on the airfoil is not identical for the 2-, 3- and 4-bladed VAWTs when operating at relatively low tip speed ratios. This can cause discrepancy in the mean value of the resultant forces. Another reason is that when the VAWTs rotate, not only the aerodynamic loads vary, so do the rotational speed and the generator torque used to regulate the rotational speed, as illustrated in Figure 7. The generator controller responds a little differently to the variation of rotational speed for VAWTs with different number of blades.

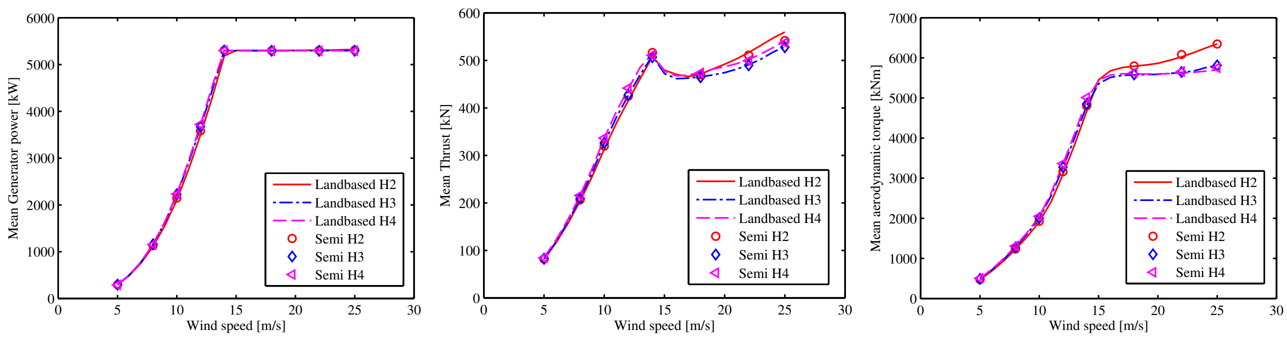

Figure 6: The mean value of the generator power, thrust and aerodynamic torque of the landbased and floating VAWTs with the improved controller.

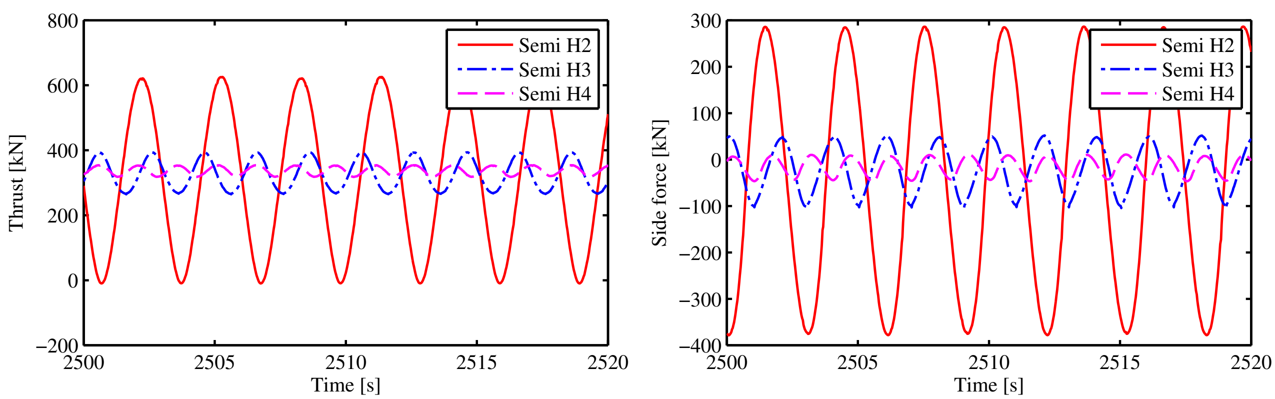

Figure 7: Time history of the thrust and side forces acting on the three floating VAWTs in the steady wind condition with a wind speed of 10 m/s.

In addition, the 2-bladed VAWT exhibits much more significant variation in the thrust and side force compared to the 3- and 4-bladed VAWTs, since its lift and drag forces of each blade reach the maximum and minimum simultaneously, causing the thrust and aerodynamic torque varying from approximate zero to double the mean value. Consequently, the induced structural responses, for instance the tower base fore-aft and side-side bending moments, vary considerably, and the fluctuation of the 2-bladed VAWT is much more notable than that of the 3- and 4-bladed VAWTs. This can be observed in Figures 7 and 8. It should also be noted that the 2-bladed floating VAWT has a larger standard deviation in pitch motion than the 3- and 4-bladed floating VAWTs, which makes its

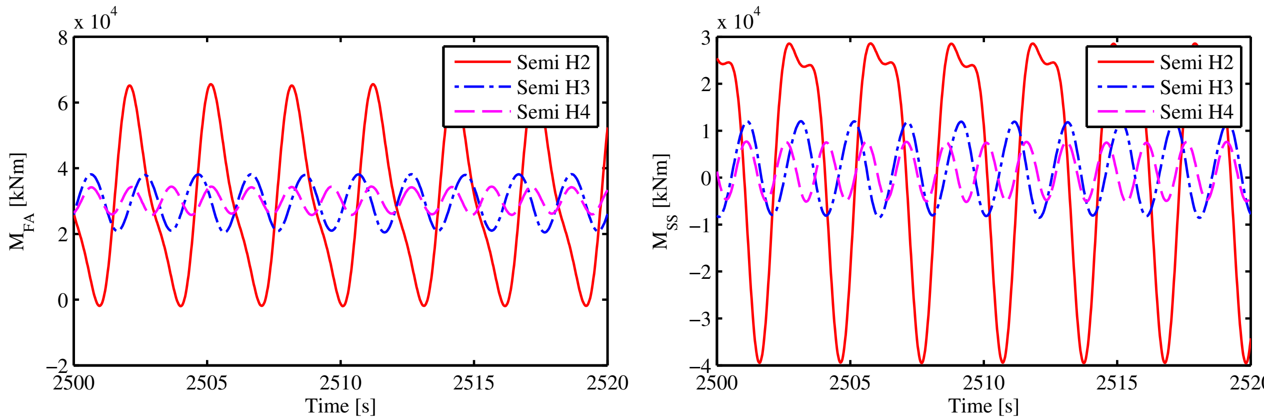

Figure 8: Time history of the tower base fore-aft and side-side bending moments of the three floating VAWTs in the steady wind condition with a wind speed of 10 m/s.

rotor weight contributing more to the variation of tower base bending moments as well.

Figure 9 further compares the mean value and standard deviation of the tower base fore-aft and side-side bending moment of the landbased and floating VAWTs in the steady wind conditions. Compared to the landbased VAWTs, the floating VAWTs give relatively larger mean value in the fore-aft bending moment, especially at high wind speeds, due to the contribution from the tower weight and platform's pitch motions. In contrast, the landbased VAWTs give larger mean value in the side-side bending moment than the floating ones. Regarding the standard deviation, both the fore-aft and side-side bending moment of the floating VAWTs are smaller than those of the landbased VAWTs. For the 2-bladed semi VAWT, the standard deviation of the fore-aft bending moment can reduce up to approximately 40% compared to the landbased one. It implies that the floating substructure with compliant catenary mooring systems can help to mitigate the variation in structural responses and thus to reduce the fatigue damage at the cost of some pitch motion. This is also demonstrated in the turbulent wind and irregular wave simulations. In addition, the 3- and 4-bladed VAWTs present much smaller standard deviations in the tower base fore-aft and side-side bending moment than the 2-bladed VAWT.

5.3 Turbulent wind and irregular wave conditions

In the turbulent wind and irregular wave conditions, several stochastic dynamic responses of the three floating VAWTs are studied, such as the wind turbine performance, platform motions, tower base bending moments and tension in mooring lines.

5.3.1 Wind turbine performance

Figure 10 shows the mean values and standard deviations of the generator power production, thrust, side force and rotor rotational speed for the three floating VAWTs in LC4. It can be found that the mean generator power production remains approximately constant above the rated wind speed (LC4.5) because of the robust controller implemented. For each LC, the difference in mean generator power among the three floating VAWTs is also very small. In addition, the mean values in the thrust and rotor rotational speed of three floating VAWTs are very close to each other for each LC as well. Although the mean side force of the 2-bladed semi VAWT is larger than those

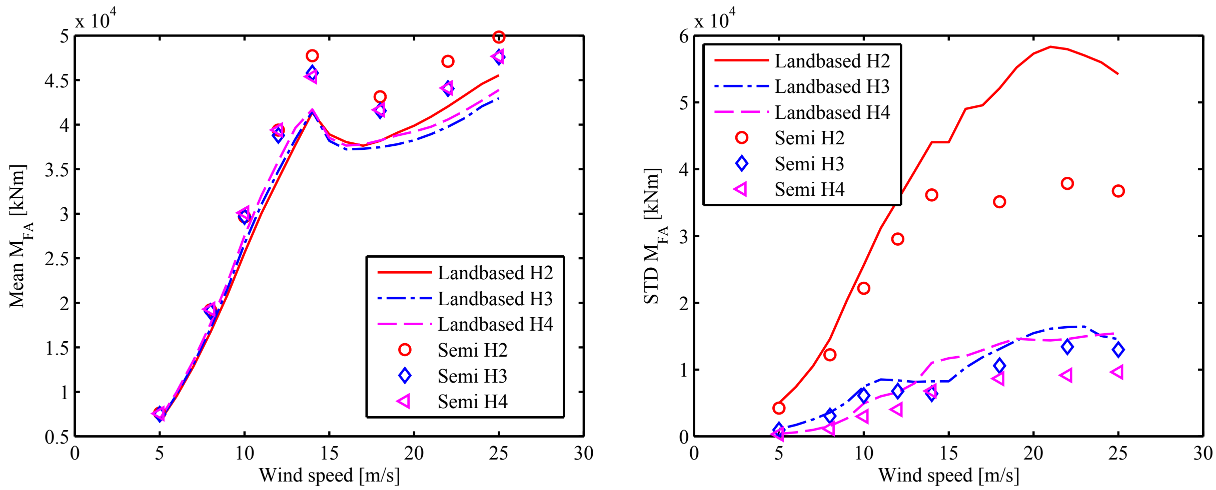

(a) Tower base fore-aft bending moment

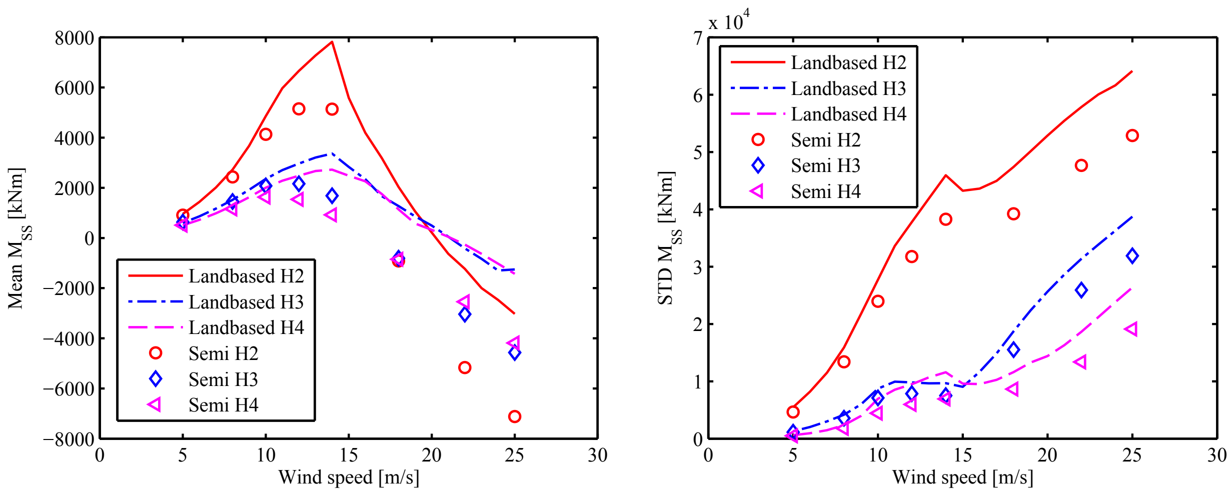

(b) Tower base side-side bending moment

Figure 9: The mean value and standard deviation of tower base fore-aft and side-side bending moments of the landbased and floating VAWTs in steady wind conditions.

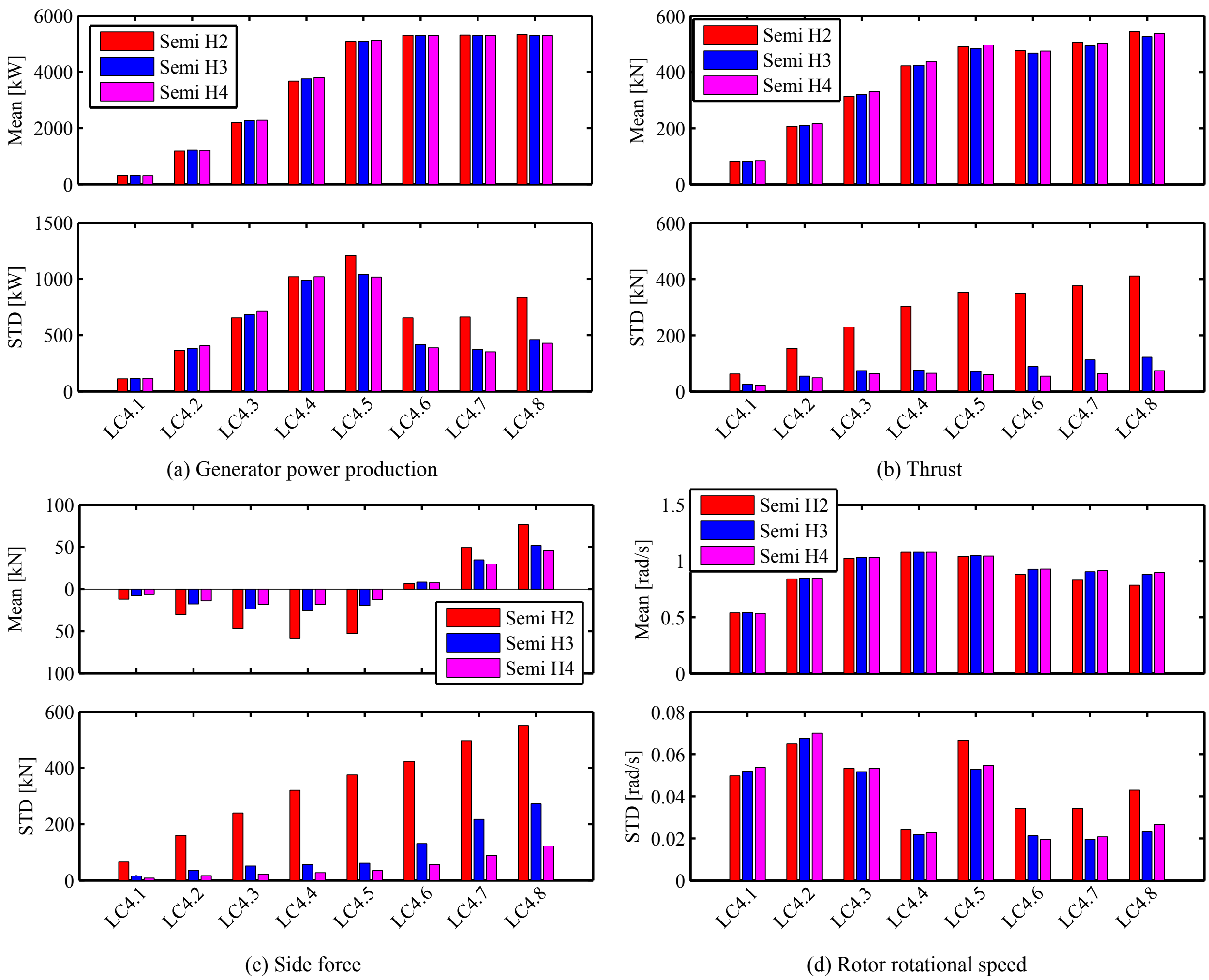

Figure 10: The mean value and standard deviation of the (a) generator power production, (b) thrust, (c) side force, and (d) rotor rotational speed of three floating VAWTs in LC4 with turbulent wind and irregular wave conditions.

of the 3- and 4-bladed semi VAWTs, the absolute value is all small compared to the mean thrust.

Visible differences in Figure 10 are observed in the standard deviations, especially in those of the thrust and side force. Such discrepancies are mainly due to the different number of blades. The blade number contributes considerably to the variation of resultant aerodynamic loads acting on the rotor, as illustrated in Figure 10 (b) and (c). The standard deviation in the thrust of the 2-bladed semi VAWT is more than three times larger than that of the 3-bladed semi VAWTs at above the wind speed of 10 m/s (LC4.3). For wind speeds ranging from the cut-in (LC4.1) to rated (LC4.5) one, the standard deviation in thrust of the 4-bladed semi VAWT is more than 80% of that of the 3-bladed semi VAWT. Regarding the side force, the 2-bladed semi VAWT gives more than four times larger standard deviation than the 3-bladed one at below the rated wind speed (LC4.5), while the standard deviation of the side force for the 4-bladed semi VAWT is approximately half of that of the 3-bladed one.

Similar to the thrust and side force, the aerodynamic torque varies significantly, especially for the 2-bladed semi VAWT. However, the fluctuation in the generator torque is relatively small compared to that of the aerodynamic torque, due to the adjustment of the controller. Consequently, the variation in the generator power is relatively small as well, as the standard deviation of the generator power shown in Figure 10. Moreover, the difference in the standard deviation of the generator power among the three semi VAWTs is much less notable than that of the aerodynamic loads. The standard deviation in the generator power of the 3- and 4-bladed semi VAWTs are very close to each other, while that of the 2-bladed semi VAWT is visibly larger than those of the 3- and 4-bladed semi VAWTs above the rated wind speed. As a whole, the generator power is not sensitive to the blade number due to the control strategy implemented.

5.3.2 Global platform motions

For the Darrieus type floating VAWTs, the mean value of platform motions are mainly induced by the wind loads (Cheng et al., 2015), this also applies to the straight-bladed floating VAWTs considered in this study, as shown in Figure 11. For all three floating VAWTs, the trends in the surge and pitch motions follow that of the thrust, while the trends in the roll and yaw motions follow that of the side force and generator torque, respectively. These three floating VAWTs have very close mean values in the aerodynamic loads, as a result their mean values in the platform motions are close to each other as well. The mean motions in surge, pitch and yaw increase as wind speeds increase. Moreover, the mean pitch and yaw motions of the 2-bladed semi VAWT are to some extent larger than those of the 3- and 4-bladed semi VAWTs above the rated wind speed.

The standard deviation of platform motions are induced by not only the wind loads but also the wave loads. It's obvious from Figure 11 that the standard deviation of platform motions of the 3- and 4-bladed semi VAWTs are generally very close to each other for each LCs. Moreover, the standard deviation of pitch motions of these three floating VAWTs are very close to each other for each LCs. However, the 2-bladed semi VAWT gives relatively larger standard deviations in surge, roll and yaw motions at LCs with wind speeds above the rated one.

Power spectral analysis was carried out to identify different contributions from the wind or wave for each mode in each LC. The power spectral results are based on only one realization for each LC. Since it has been stated in section 5.1 that these three floating VAWTs have almost identical RAOs in surge and heave motions when subjected to wave loads, the discrepancy in the standard deviation of surge motions are mainly caused by the wind loads. Figure 12 presents the power spectra of surge motions in LC4.2 and LC4.7. The wave frequency response of these

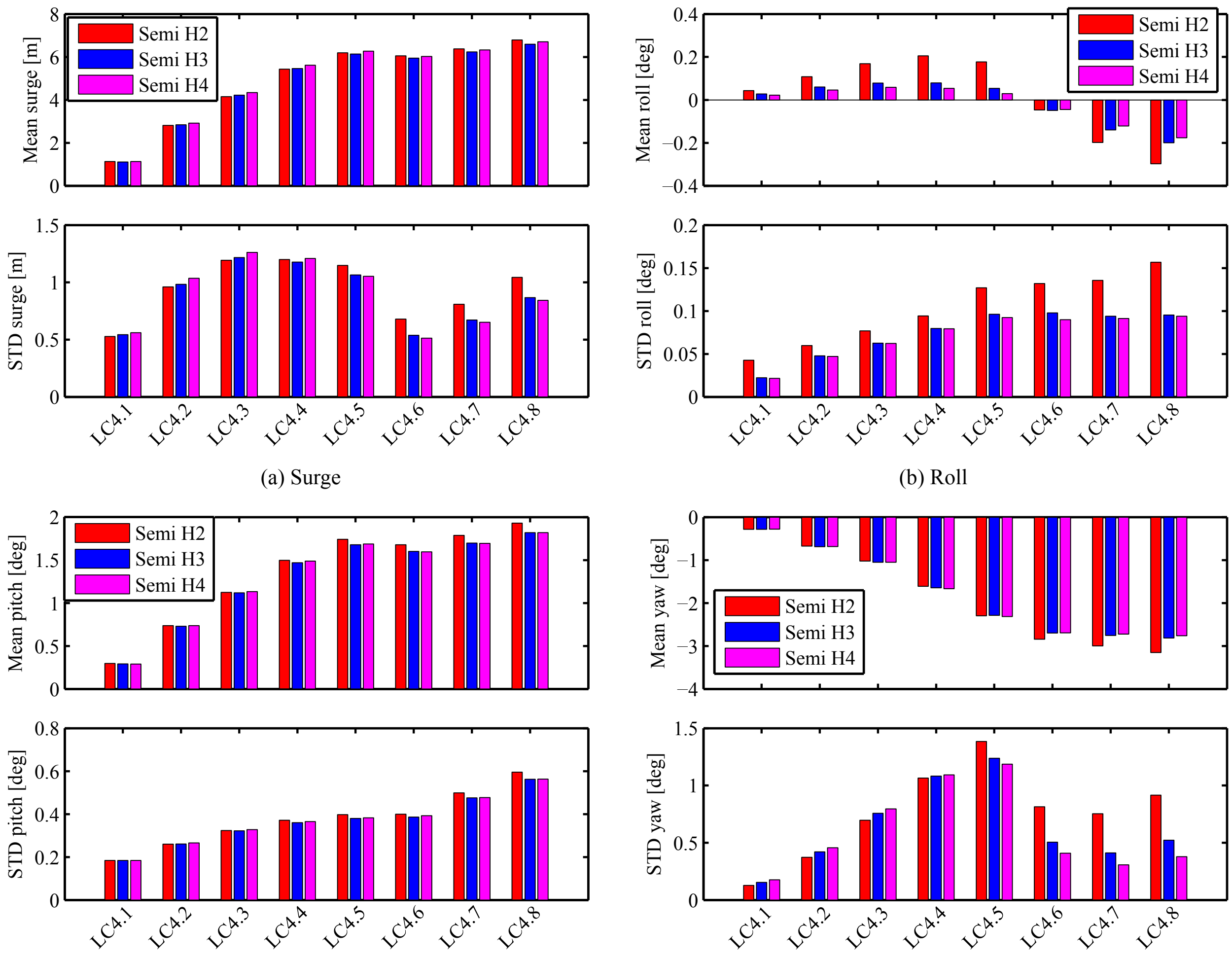

(a) Surge (b) Roll

(c) Pitch (d) Yaw

Figure 11: The mean values and standard deviations of the surge, roll, pitch and yaw motions of three floating VAWTs in LC4 with turbulent wind and irregular wave conditions.

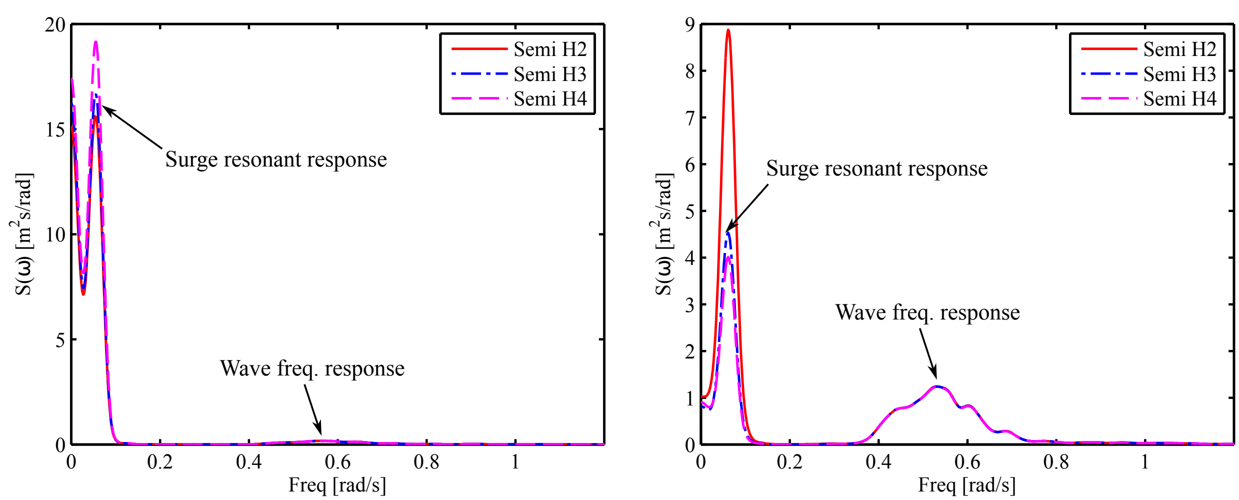

(a) LC4.2: Uw=8m/s, Hs=2.55m, Tp=9.74s (b) LC4.7: Uw=22m/s, Hs=5.32m, Tp=11.06s

Figure 12: Power spectra of the surge motion of three floating VAWTs in (a) LC4.2 and (b) LC4.7.

three floating VAWTs are identical and the difference in responses locates at the surge resonant frequency. The 2-bladed semi VAWT has slightly smaller surge resonant response at LCs with wind speeds below the rated one, while it holds a little larger surge resonant response at LCs with wind speeds above the rated one. Moreover, no 2P, 3P or 4P response is observed in the power spectra of surge motions for the 2-, 3- and 4-bladed semi VAWT, respectively. In addition, the more severe the sea state is, the more the wave loads contribute to the surge power spectra.

Power spectra of pitch motions in Figure 13 (b) reveal that the contributions are from the low turbulent wind induced response, pitch resonant response and wave frequency response. In a very severe sea state such as LC4.7 and LC4.8, a very small 2P response is also observed only for the 2-bladed semi VAWT. Due to the identical RAOs in the range of wave frequency, the wave frequency pitch response is also almost identical for these three floating VAWTs. Moreover, Pitch response with contribution from wave loads increases as the sea state becomes more severer, which is similar as the surge response. Regarding the power spectra of roll motions, not only is a notable 2P response observed for the 2-bladed semi VAWT, but also a very small 3P response is captured for the 3-bladed semi VAWT. However, no 4P response is identified for the 4-bladed semi VAWT.

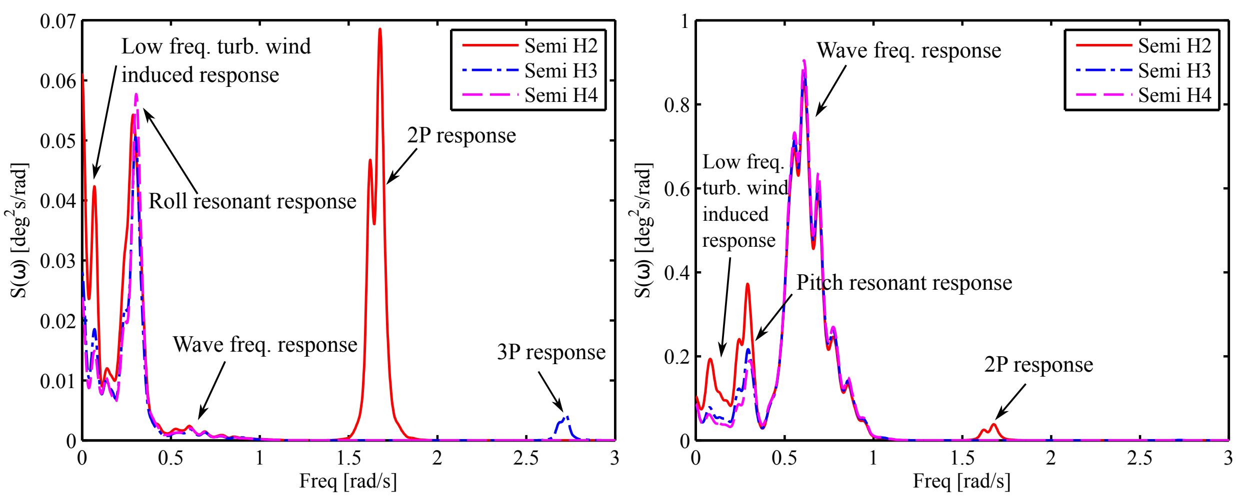

(a) Roll in LC4.7: Uw=22m/s, Hs=5.32m, Tp=11.06s (b) Pitch in LC4.7: Uw=22m/s, Hs=5.32m, Tp=11.06s

Figure 13: Power spectra of the (a) roll motion and (b) pitch motion of three floating VAWTs in LC 4.7.

The power spectra of yaw motions are mainly dominated by the low turbulent wind induced response and yaw resonant response, as shown in Figure 14. At LCs with wind speeds below the rated one, the 4-bladed semi VAWT gives a litter larger yaw resonant response; while it presents much smaller yaw resonant response at LCs with wind speeds above the rated one.

5.3.3 Tower base bending moments

It is of great interest to study the effect of blade number on the structural response. In this study the tower base bending moment was considered. The tower base bending moment is usually caused by the aerodynamic loads acting on the rotor as well as by the mass of the rotor due to the platform's pitch and roll motions.

Figure 15 compares the mean value and standard deviation of the tower base for-aft bending moment M_{FA}

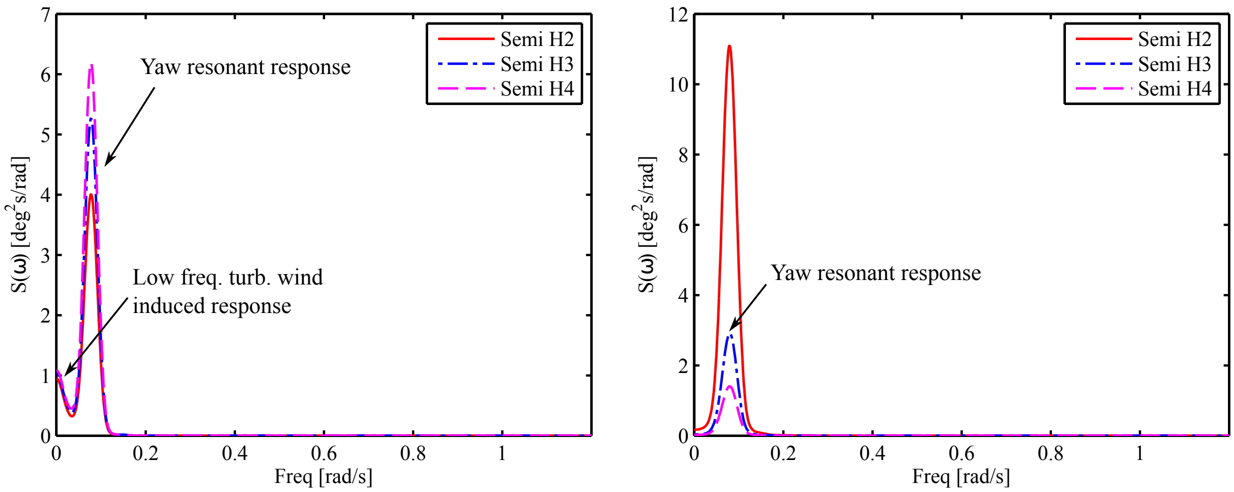

(a) LC4.2: Uw=8m/s, Hs=2.55m, Tp=9.74s

(b) LC4.7: Uw=22m/s, Hs=5.32m, Tp=11.06s

Figure 14: Power spectra of the yaw motion of three floating VAWTs in (a) LC4.2 and (b) LC4.7.

and side-side bending moment M_{SS} for the three floating VAWTs in LC4. Obviously the discrepancy in the mean value of both M_{FA} and M_{SS} for the three floating VAWTs is fairly small, and is much less notable than that in the standard deviation. This is due to two possible reasons: one is that the mean value of the aerodynamic loads acting on the rotor is very close to each other, and the torque arm resulting in the tower base bending moments is almost identical. Another reason is that these three floating VAWTs slightly differ in the rotor mass, and in the mean value of the pitch and roll motions of the platform since the pitch and roll motions are mainly wind-induced.

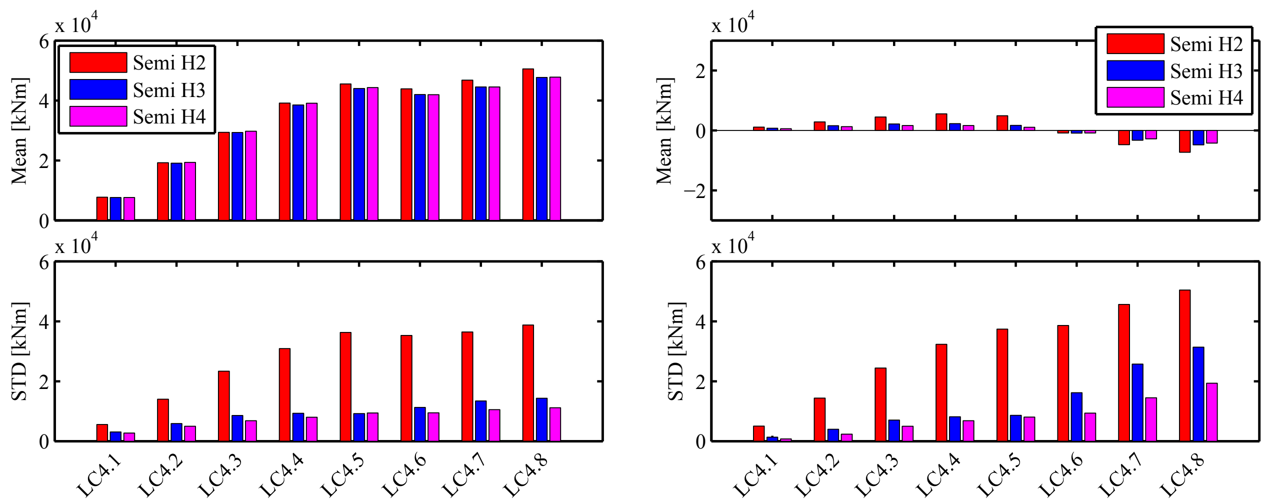

(a) Tower base fore-aft bending moment

(b) Tower base side-side bending moment

Figure 15: The mean value and standard deviation of tower base fore-aft and side-side bending moments of three floating VAWTs in LC4 with turbulent wind and irregular wave conditions.

The 2-bladed semi VAWT gives significantly larger standard deviation than the 3- and 4-bladed semi VAWTs with respect to both the M_{FA} and M_{SS}, as illustrated in Figure 15. The ratio of the standard deviation of the 2-bladed semi VAWT to that of the 3-bladed semi VAWT varies from 2.37 to 3.93 for LC4.2-LC4.7, while the ratio of the standard deviation of the 4-bladed semi VAWT to that of the 3-bladed semi VAWT remains approximately constant at 0.8. It indicates that increasing blade number from 2 to 3 blades can decrease M_{FA} more significantly than increasing blade number from 3 to 4 blades. A similar conclusion can also be drawn for the M_{FA}. In addition, it is also interesting to see that for the 2-bladed semi VAWT the M_{FA} is smaller than the M_{SS} for all LCs except LC4.1, and the discrepancy between M_{FA} and M_{SS} can reach more than 20% at LC4.7 and LC4.8. But both 3- and 4-bladed semi VAWT predict to some extent larger M_{FA} than M_{SS} in LCs with wind speed at or below the rated one.

Power spectral analysis can be used to identify the different contributions to the variation of the M_{FA} and M_{SS}, as shown in Figure 16. These three floating VAWTs have very close low frequency turbulent wind induced response and wave frequency response, as well as noticeable different responses at the nP (2P, 3P and 4P) frequency. Moreover, the nP response is increasingly dominating, especially in LCs with high wind speeds. For the 2-bladed semi VAWT, it is seen that not only is the 2P response significant but even the 4P response is visible, while only 3P and 4P response is captured for the 3- and 4-bladed semi VAWT, respectively.

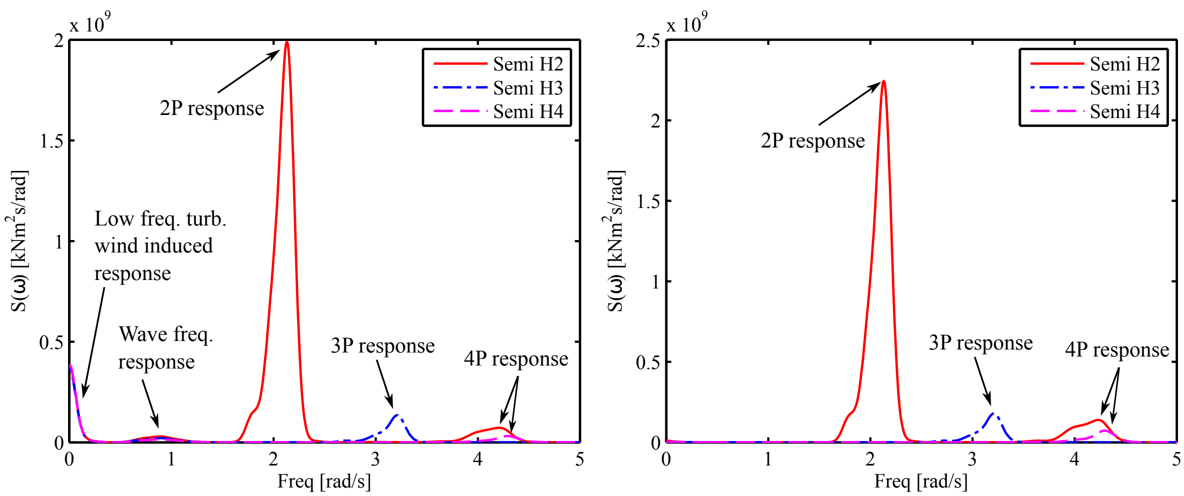

(a) Tower base fore-aft bending moment (b) Tower base side-side bending moment

Figure 16: Power spectra of the (a) tower base fore-aft bending moment and (b) side-side bending moment of three floating VAWTs in LC4.3

5.3.4 Tension in mooring lines

Identical catenary mooring systems with three mooring lines were use to keep the three floating VAWTs in position. The layout of the mooring system is given by Robertson et al. (2012). Among the three mooring lines, the mooring line 2 is in line with the wind and wave directions and carries the largest tension when the floating VAWTs are subjected to the wind and wave loads. The tension in mooring line 2 is thus studied.

Figure 18 shows the mean value and standard deviation of the tension in mooring line 2 of the three floating VAWTs in LC4. It can be found that the mean value for each LC is very close to each other for the three floating VAWTs and visible difference is only observed in the standard deviation, especially in LCs with wind speed at or above the rated one. Moreover, the standard deviation is relatively small compared with the mean value, implying that the present mooring system could be sufficient even in survival conditions.

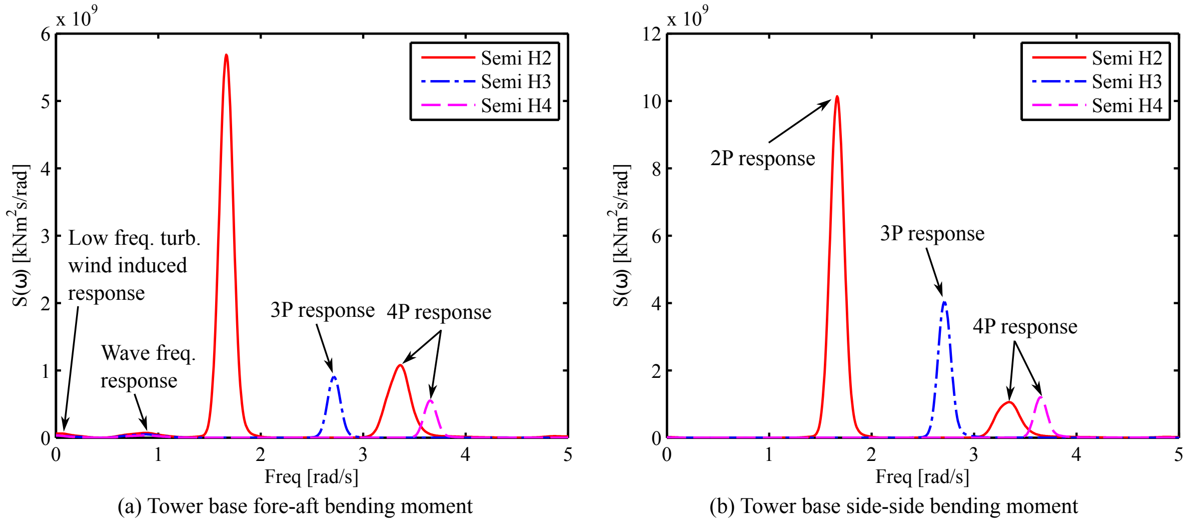

Figure 17: Power spectra of the (a) tower base fore-aft bending moment and (b) side-side bending moment of three floating VAWTs in LC4.7

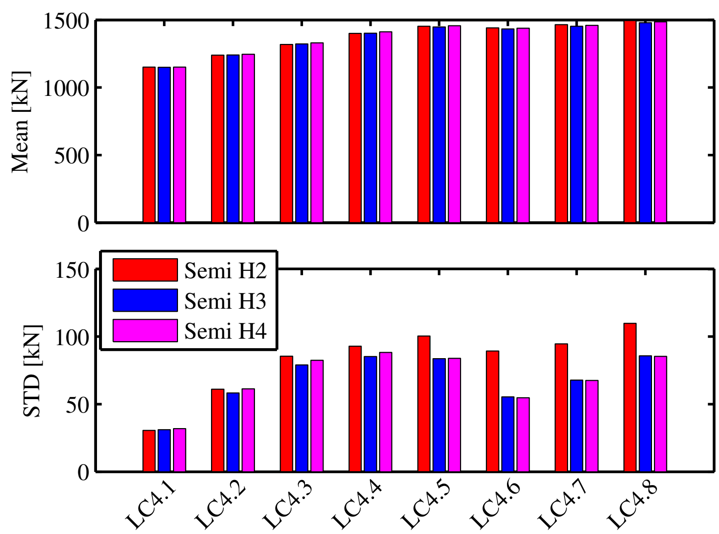

Figure 18: The mean value and standard deviation of the tension in mooring line 2 of three floating VAWTs in LC4 with turbulent wind and irregular wave conditions.

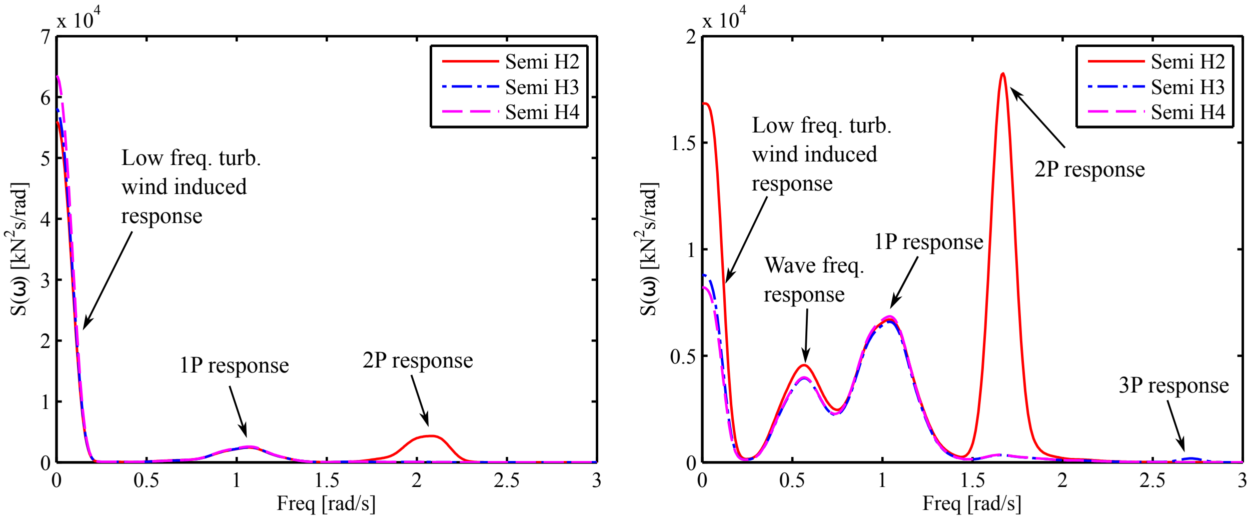

(a) LC4.3: Uw=10 m/s, Hs=2.88 m, Tp=9.98 s (b) LC4.7: Uw=22 m/s, Hs=5.32 m, Tp=11.06 s

Figure 19: Power spectra of the tension in mooring line 2 of three floating VAWTs in (a) LC4.3 and (b) LC4.7.

The difference in the standard deviation can be explored by using the power spectra analysis. Figure 19 gives the power spectra of tension in mooring line 2 of the three floating VAWTs for LC4.3 and LC4.7. Generally the power spectral density is dominated by the low frequency turbulent wind induced response and 1P response for the three floating VAWTs; and the wave frequency response also becomes dominating at LCs with high significant wave height. For the 2-bladed semi VAWT the 2P response is also very prominent, especially at LCs with high wind speed. In addition, a very small 3P response is also captured for the 3-bladed semi VAWT in LC4.7 and LC4.8. But no 4P response for the 4-bladed semi VAWT is observed for all LCs. In LC4.2 to LC4.4, the 2-bladed semi VAWT gives the largest standard deviation of tension in mooring line 2 because of the 2P response; while in LC4.5 to LC4.8, not only considerably large 2P response but also the low frequency turbulent wind induced response contribute to the standard deviation, causing it much larger compared to those of the 3- and 4-bladed semi VAWTs.

6 Conclusions

This study deals with the effect of the number of blades on the dynamic behavior of floating vertical axis wind turbines (VAWTs) with straight parallel blades. Three straight-bladed VAWTs with identical solidity and with a blade number ranging from two to four were aerodynamically designed using the actuator cylinder flow method. These three VAWTs were then adapted to a semi-submersible platform to establish three floating straight-bladed VAWTs, which have identical draft and displacement and use the same mooring system. A generator torque controller was also designed and used to regulate the rotational speed based on a proportional-integral (PI) control algorithm.

The dynamic response of the floating VAWTs was then computed based on a series of load cases using the fully coupled aero-hydro-servo-elastic simulation tool SIMO-RIFLEX-AC. The floating VAWT systems were firstly identified using the eigen-frequency analysis, free decay tests and white noise wave simulations. The natural periods of rigid-body motions and response amplitude operators (RAOs) in surge, pitch and heave are all close to each other for the three floating VAWTs.

Steady wind simulations capture the effect of the number of blades on the structural responses of the landbased and floating VAWTs. Floating substructures with a compliant mooring system can help to alleviate the variations in the structural responses, for instance in the tower base fore-aft and side-side bending moment. The tower base fore-aft bending moment, especially for the 2-bladed floating VAWT, can be greatly reduced above the rated wind speed, compared to that of the corresponding equivalent landbased one.

The impact of the number of blades is further studied using the turbulent wind and irregular wave simulations. Stochastic dynamic response analysis shows that the variation of aerodynamic loads such as the thrust and side force are strongly dependent on the number of blades; consequently the standard deviation of structural responses for instance the tower base bending moment is significantly influenced, which implies that the fatigue damage is reduced. Moreover, increasing the number of blades from two to three can significantly decrease the variation in the tower base bending moments and hence reduce the fatigue damage, whereas increasing from three to four blades has limited additional effect. However, the generator power production is not sensitive to the number of blades due to the control strategy used. The proposed control strategy is slightly more suitable for the 3- and 4-bladed floating VAWT. Moreover, neither the platform motions nor mooring line tension are very sensitive to the number of blades either because of the compliant catenary mooring system.

As a whole, this study demonstrates the effect of the number of blades on the dynamic behavior of floating VAWTs using a fully coupled aero-hydro-servo-elastic approach and will serve as a basis for the preliminary design trade-offs with respect to the number of blades for floating VAWTs.

Acknowledgement

The authors would like to acknowledge the financial support from the EU FP7 project MARE WINT (project NO. 309395) and the Research Council of Norway through the Centre for Ships and Ocean Structures (CeSOS) and Centre for Autonomous Marine Operations and Systems (AMOS) at the Department of Marine Technology, Norwegian University of Science and Technology (NTNU), Trondheim, Norway.

References

Anagnostopoulou, C., Kagemoto, H., Sao, K., Mizuno, A., 2015. Concept design and dynamic analyses of a floating vertical-axis wind turbine: case study of power supply to offshore greek islands. Journal of Ocean Engineering and Marine Energy 2 (1), 85–104.

Bachynski, E. E., 2015. Design and dynamic analysis of tension leg platform wind turbines. PhD thesis, Norwegian University of Science and Technology.

Bedon, G., Schmidt Paulsen, U., Aagaard Madsen, H., Belloni, F., Raciti Castelli, M., Benini, E., 2015. Computational assessment of the deepwind aerodynamic performance with different blade and airfoil configurations. Applied Energy.

Borg, M., Collu, M., 2015. Frequency-domain characteristics of aerodynamic loads of offshore floating vertical axis wind turbines. Applied Energy 155, 629–636.

Borg, M., Collu, M., Brennan, F. P., 2013. Use of a wave energy converter as a motion suppression device for floating wind turbines. Energy Procedia 35, 223–233.

Borg, M., Manuel, L., Collu, M., Liu, J., 2015. Long-term global performance analysis of a vertical-axis wind turbine supported on a semi-submersible floating platform. In: ASME 2015 34th International Conference on Ocean, Offshore and Arctic Engineering. American Society of Mechanical Engineers, p. V009T09A066.

Brusca, S., Lanzafame, R., Messina, M., 2014. Design of a vertical-axis wind turbine: how the aspect ratio affects the turbine's performance. International Journal of Energy and Environmental Engineering 5 (4), 333–340.

Cahay, M., Luquiau, E., Smadja, C., Silvert, F., 2011. Use of a vertical wind turbine in an offshore floating wind farm. In: Offshore Technology Conference. Houston, Texas, USA.

Cheng, Z., Madsen, H. A., Gao, Z., Moan, T., 2016a. Aerodynamic modeling of offshore vertical axis wind turbines using the actuator cylinder method. Energy Procedia.

Cheng, Z., Madsen, H. A., Gao, Z., Moan, T., 2016b. A fully coupled method for numerical modeling and dynamic analysis of floating vertical axis wind turbines. Submitted to Renewable Energy.

Cheng, Z., Wang, K., Gao, Z., Moan, T., 2015. Dynamic response analysis of three floating wind turbine concepts with a two-bladed darrieus rotor. Journal of Ocean and Wind Energy 2, 213–222.

Cheng, Z., Wang, K., Gao, Z., Moan, T., 2016c. A comparative study on dynamic responses of spar-type floating horizontal and vertical axis wind turbines. Wind Energy.

Collu, M., Brennan, F. P., Patel, M. H., 2014. Conceptual design of a floating support structure for an offshore vertical axis wind turbine: the lessons learnt. Ships and Offshore Structures 9 (1), 3–21.

Dabiri, J. O., 2011. Potential order-of-magnitude enhancement of wind farm power density via counter-rotating vertical-axis wind turbine arrays. Journal of Renewable and Sustainable Energy 3 (4), 043104.

Faltinsen, O. M., 1995. Sea loads on ships and offshore structures. Cambridge University Press, Cambridge, UK.

Ferreira, C. S., Madsen, H. A., Barone, M., Roscher, B., Deglaire, P., Arduin, I., 2014. Comparison of aerodynamic models for vertical axis wind turbines. Journal of Physics: Conference Series 524 (1), 012125.

IEC, 2005. International standard 61400-1, wind turbines, part 1: Design requirements.

Johannessen, K., Meling, T. S., Haver, S., 2002. Joint distribution for wind and waves in the northern north sea. International Journal of Offshore and Polar Engineering 12 (1).

Jonkman, B. J., 2009. Turbsim user's guide: Version 1.50.

Jonkman, J. M., Butterfield, S., Musial, W., Scott, G., 2009. Definition of a 5-mw reference wind turbine for offshore system development. Tech. Rep. NREL/TP-500-38060, NREL, Golden, CO, USA.

Li, Q., Maeda, T., Kamada, Y., Murata, J., Furukawa, K., Yamamoto, M., 2015. Effect of number of blades on aerodynamic forces on a straight-bladed vertical axis wind turbine. Energy 90, 784–795.

Madsen, H. A., 1982. The Actuator Cylinder: A flow model for vertical axis wind turbines. Institute of Industrial Constructions and Energy Technology, Aalborg University Centre.

Madsen, H. A., Larsen, T. J., Paulsen, U. S., Vita, L., 2013. Implementation of the actuator cylinder flow model in the HAWC2 code for aeroelastic simulations on vertical axis wind turbines. In: 51st AIAA Aerospace Sciences Meeting including the New Horizons Forum and Aerospace Exposition.

MARINTEK, 2012a. Riflex theory manual, version 4.0.

MARINTEK, 2012b. Simo-theory manual version 4.0.

Merz, K. O., Svendsen, H. G., 2013. A control algorithm for the deepwind floating vertical-axis wind turbine. Journal of Renewable and Sustainable Energy 5 (6), 063136.

Paquette, J., Barone, M., 2012. Innovative offshore vertical-axis wind turbine rotor project. In: EWEA 2012 Annual Event. Copenhagen, Denmark.

Paraschivoiu, I., 2002. Wind turbine design: with emphasis on Darrieus concept. Polytechnic International Press., Montreal, Canada.

Paulsen, U. S., Borg, M., Madsen, H. A., Pedersen, T. F., Hattel, J., Ritchie, E., Ferreira, C. S., Svendsen, H., Berthelsen, P. A., Smadja, C., 2015. Outcomes of the deepwind conceptual design. Energy Procedia 80, 329–341.

Robertson, A., Jonkman, J., Masciola, M., Song, H., Goupee, A., Coulling, A., Luan, C., 2012. Definition of the semi-submersible floating system for phase II of OC4. Report.

Wang, K., Cheng, Z., Moan, T., Hansen, M. O. L., 2015. Effect of difference-frequency forces on the dynamics of a semi-submersible type FVAWT in misaligned wave-wind condition. In: Proceedings of the 25th International Ocean and Polar Engineering Conference.

Wang, K., Hansen, M. O. L., Moan, T., 2014. Dynamic analysis of a floating vertical axis wind turbine under emergency shutdown using hydrodynamic brake. Energy Procedia 53, 56–69.

Wang, K., Moan, T., Hansen, M. O. L., 2013. A method for modeling of floating vertical axis wind turbine. In: Proceedings of the 32th International Conference on Ocean, Offshore and Arctic Engineering.

Wang, K., Moan, T., Hansen, M. O. L., 2016. Stochastic dynamic response analysis of a floating vertical-axis wind turbine with a semi-submersible floater. Wind Energy.